J. Am. Soc. Mass Spectrom. (2013)
DOI: 10.1007/s13361-012-0559-8

RESEARCH ARTICLE

Overtone Mobility Spectrometry: Part 5. Simulations and Analytical Expressions Describing Overtone Limits

Michael A. Ewing,[1] Steven M. Zucker,[1] Stephen J. Valentine,[1,2] David E. Clemmer[1]

[1]Department of Chemistry, Indiana University, Bloomington, IN 47405, USA
[2]Department of Chemistry, West Virginia University, Morgantown, WV 26506, USA

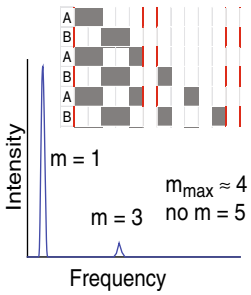

Abstract. Mathematical expressions for the analytical duty cycle associated with different overtones in overtone mobility spectrometry are derived from the widths of the transmitted packets of ions under different instrumental operating conditions. Support for these derivations is provided through ion trajectory simulations. The outcome of the theory and simulations indicates that under all operating conditions there exists a limit or maximum observable overtone that will result in ion transmission. Implications of these findings on experimental design are discussed.

Key words: Ion mobility spectrometry, Overtone mobility spectrometry, Mass spectrometry

Received: 5 September 2012/Revised: 4 December 2012/Accepted: 5 December 2012

Introduction

Ion mobility spectrometry (IMS) coupled with mass spectrometry (MS) provides a powerful means of analyzing complex samples such as those encountered in proteomics [1, 2], glycomics [3, 4], and petroleomics [5, 6] studies. Of particular interest is the ability to select ions based on their shapes (or mobilities) and use this information to complement structural information derived from MS experiments [7, 8]. While traditional IMS has enjoyed a resurgence in popularity, limitations in achieving very high resolving powers spawned the development of a range of related techniques, such as traveling wave ion mobility spectrometry (TWIMS) [9–12], differential mobility analysis (DMA) [13–15], field asymmetric waveform ion mobility spectrometry (FAIMS) [16–19], and overtone mobility spectrometry (OMS) [20–24]. The latter three methods act as selective filters for desired ions and are capable of very high resolving powers [19, 22] whereas the former is more analogous to conventional IMS in that ions are temporally dispersed. OMS shows limited similarity to TWIMS with both using a pulsed sequence of applied potentials, each of which repeats in space along the length of the drift tube. As opposed to TWIMS, in OMS certain ions are eliminated instead of separated by the wave, leading to a change in the overall mechanism of separation reflected in the resolving power equation. Effectively, this process reduces the ability of ions that have either diffused away or are mobility mismatched to diffuse back towards the center of a mobility-matched ion swarm [20, 21]. The preferential elimination of ions whose mobility does not match the field application frequency results in a very different technique with an increased potential for garnering high resolving power compared with traditional IMS [20, 21] and TWIMS. As related to TWIMS in the use of alternating fields, OMS may also provide a greater understanding of the former technique. For example, an increased understanding of mobility matching requirements may aid TWIMS experimental design particularly for the separation of high mobility species, as often such ions are observed to travel at the wave velocity. Finally, it is noted that OMS is distinguished from TWIMS in that a true collision cross section can be determined from OMS measurements, whereas the TWIMS approach requires a calibration method.

One interesting aspect of OMS is that the technique can be used to transmit ions having specific mobilities (and these mobilities can be compared directly to theory as a means of determining structure, as in traditional IMS). The use of an entrance and exit gate in IMS in a scanning mode yields the limiting case of OMS—one segment—and the use of multiple segments to improve resolving power scaling has been discussed previously [20, 21]. The observation that ions can be transmitted at multiples of the fundamental frequency (i.e., in overtone regions of the spectrum) presents opportunities to explore transitions between structures in a

Electronic supplementary material The online version of this article (doi:10.1007/s13361-012-0559-8) contains supplementary material, which is available to authorized users.

Correspondence to: David E. Clemmer; *e-mail:* Clemmer@Indiana.EDU

Published online: 07 March 2013

new way [22]. Experimentally it is observed that beyond a certain overtone no additional ions are transmitted [20–24]. It is of interest to understand the origin of this limit. In this paper, we present mathematical expressions for the analytical duty cycle associated with different overtones for a range of possible experimental conditions. This theoretical treatment is supported by detailed ion trajectory simulations. The outcome is an understanding of the maximum overtone that can still transmit ions for a given experiment.

In the treatment presented below, we assume an OMS configuration based on a series of Tyndall gates [25] although this is not required. A uniform spacing between gates along with a uniform electric field yields a direct correspondence between the mobility of the selected ions and the drift field application frequency, which is the frequency of application of a defined number of different fields, ϕ [20, 21]. Overtones appear where ions traverse a single segment in the same time, but at a field application frequency that is some multiple of the fundamental frequency, m, known as the OMS frequency coefficient. These overtones have the same peak width as the fundamental frequency but with higher frequencies and, thus, a higher resolving power [20]. For higher numbers of phases (ϕ>2), there also exist higher order overtone series with different bandwidths, which can exist at non-integer multiples of the fundamental frequency [23].

Experimental Simulations

For background, it is helpful to understand theoretical and experimental issues that are associated with IMS, as have been described previously [26–36]. Simulations of ion motion through a gas were performed using a program written in house that is similar to others [21–23, 37–39] with differences noted below. Briefly, electric fields were calculated using SIMION 8.0 [40] and those fields were used as inputs for the simulation program. The simulations were performed by moving all ions simultaneously through the applied field. Ion motion for each time step was determined from the sum of the electric field-directed motion and the Brownian motion obtained from a Gaussian distribution with the standard deviation of $\sqrt{2Dt}$ in each dimension, where D is the diffusion coefficient and t is the time step, as described by Mason and McDaniel [26]. The locations of grids where ions could potentially be eliminated were read into the program independently. As fields alternated, the possibility of a grid acting to neutralize ions as an elimination region was determined by whether each grid contained a local potential minimum. A detector was placed at the end of the drift tube and any ion that entered the detector was neutralized and added to the count of signal. A separate simulation was run for each field application time, the time for which a field was applied before transitioning to the next applied field (OMS phase). The frequency was scanned by running simulations at a range of field application times.

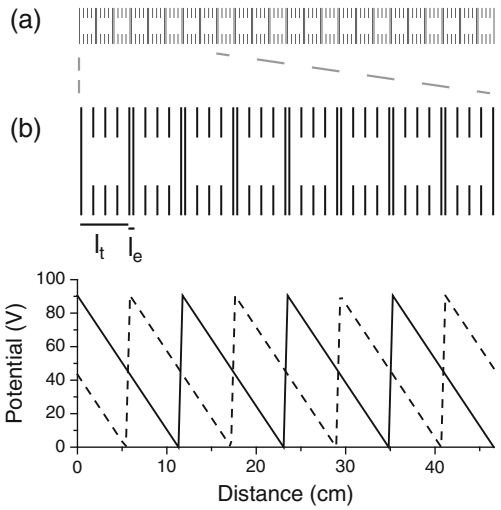

Figure 1. **(a)** Instrument schematic of the 141 cm drift tube used in simulations performed throughout this work. Lenses and grids in black. Lenses that do not break across the axis of the instrument (horizontal line bisecting the lenses) are modeled as 100 % transmittance grids. **(b)** Enlarged schematic of one-third of drift tube (47 cm) along with corresponding applied potentials. Solid and dashed lines represent two phases of applied potentials for ϕ=2. Phases are alternated during simulation at times corresponding to the drift field application frequency

For all of the simulations performed below, a schematic representing the instrument geometry is presented in Figure 1 along with the applied electric potentials for the two-phase simulations. Four-phase simulations similarly cycle through four sets of applied potentials, each of which spatially repeats every four segments. Simulations used a transmission region length (l_t) of 5.38 cm, an elimination region length (l_e) of 0.50 cm, n (number of segments) of 24, and an 8 V/cm field. Ions of the Substance P peptide with a +2 charge and a reduced mobility of 3.41 $cm^2V^{-1}s^{-1}$ [41] were simulated at a pressure of 2.25 Torr and a temperature of 298 K.

For two-phase simulations, the field application time was scanned across peaks in increments to obtain several data points across the peak. All inputs to the program are in field application times and all conversions to frequency are performed after simulations are completed. For all simulations, the field application time was scanned in order to find the maximum signal in a peak across ranges for various peaks. Values of field application time for two phase simulations were scanned (all values in μs) from 51.00 to 53.00 and from 66.00 to 68.00 in increments of 0.02, from 91.6 to 96.0 in increments of 0.1, 150.0 to 161.0 in increments of 0.2, and from 370.0 to 570.0 in increments of 2.0. Simulations were done with 100,000 ions and a time step of 0.1 μs for all OMS phase lengths above 90 μs and 1,000,000 ions and a time step of 0.01 μs for all OMS phase lengths below 90 μs.

For the four-phase simulations, the field application time (all values in μs) was scanned from 10.0 to 70.0 in increments of 0.1, 70.0 to 100.0 in increments of 0.2,

100.0 to 370.0 in increments of 0.5, and 370.0 to 570.0 in increments of 1.0. All simulations were performed with 100,000 ions and a time step of 0.1 μs.

To ensure that an entire set of repeating segments was filled, starting positions of ions were equally spaced across the first two segments for two-phase simulations and across the first four segments for four-phase simulations, leading to 1000 unique ion positions for two-phase simulations and 2000 unique ion positions for four-phase simulations.

Results and Discussion

Stable Region Length

In OMS, a beam of ions transmits down the potential gradient of a drift tube and portions of this beam are eliminated when elimination regions become active. This results in packets of ions that traverse the drift tube and are eventually detected spaced between void regions that do not contain to-be-detected ions. We define the transmitting packet as a contiguous collection of ions from which currently transmitting ions would continue to transmit if the dispersive effect of diffusion was ignored. We then define the stable region as the region occupied by the transmitting packet at a phase change. For two-phase OMS, the stable region length (l_{stable}) can be seen as the segment length ($l_t + l_e$) divided by the OMS frequency coefficient, m, if the effect of length of the elimination region on the loss of ions is ignored. As shown by the schematic in Figure 2 and observed in the simulation snapshot provided in Figure 2, the size of the elimination region subtracts from the segment length divided by the OMS frequency coefficient, resulting in Equation (1). This can be understood to be equivalent to that described by and results directly in the expression derived to describe OMS resolving power when the dispersive effect of diffusion is not included [21].

$$l_{stable} = \frac{(l_t + l_e)}{m} - l_e \tag{1}$$

To extend this expression to higher numbers of phases, we examine the stable regions for higher numbers of phases and higher order overtone series. Analysis of the patterns we observe from Table 1 for the primary overtone series yields the realization that the length of the stable region unaffected by the elimination length is $(\phi-1)$ divisions followed by one division affected by the elimination region, where each division is sized such that ϕ divisions repeat m times in ϕ segments. Thus, for the primary overtone series of higher phases, as the elimination region increases in size, the stable region length can be separated into two terms. The first of these is the length of ϕ segments minus those portions of the beam that are prohibited from transmitting (seen as void regions between transmitting packets), all divided by m. The second of these is the loss of ions

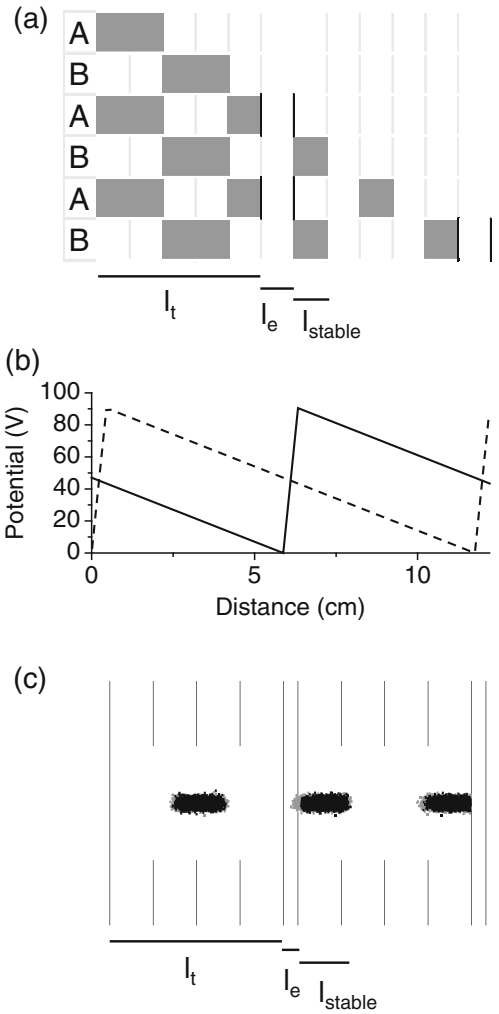

Figure 2. **(a)** Schematic demonstrating the loss of a portion of the transmitting packet equivalent to the length of the elimination region for a two-phase system with m=3. Gray blocks represent transmitting ions with white space representing locations with no ions. A and B along the left of each line represent the phase starting when ions are at the location indicated. Dark black lines border active elimination regions, light gray lines aid the reader in equal distance (one-fifth of l_t and equal to the length l_e) steps through segments of the instrument. Ions enter from the left and travel one-third of the segment length for each phase. **(b)** Potentials as applied to the corresponding simulation, vertically lined up to indicate where ions are eliminated. Solid is phase A, dashed is phase B. **(c)** Snapshot of current ion location at 936 μs for a simulation with a 156 μs field application time. Transmitting packet ions are black squares and other currently surviving ions that will be eliminated before reaching the detector are gray squares. The gray squares on the left of the middle of three packets are ions that have diffused out from the previously defined transmitting packet and are about to be eliminated in the elimination region in the middle of the figure. In the microseconds leading up to this snapshot, a similar set of ions that was on the right side of the right-most packet was eliminated as it encountered the elimination region on the far right of the figure

Table 1. Summary of Packet Characteristics As Derived From Schematics, Examples of Which Are Shown In The Supplemental Information

ϕ	k	q	m	l_{stable}[a]	Length unoccupied[b]	Duty cycle
4	1	1	2.33	1/7	3/7	1/4
4	1	2	3.67	1/11	3/11	1/4
4	1	4	6.33	1/19	3/19	1/4
4	1	5	7.67	1/23	3/23	1/4
4	2	1	3	2/6	2/6	2/4
4	2	3	7	2/14	2/14	2/4
4	2	5	11	2/22	2/22	2/4
4	3	0	1	3/1	1/1	3/4
4	3	1	5	3/5	1/5	3/4
4	3	2	9	3/9	1/9	3/4
4	3	3	13	3/13	1/13	3/4
6	1	1	2.2	1/11	5/11	1/6
6	1	2	3.4	1/17	5/17	1/6
6	1	3	4.6	1/23	5/23	1/6
6	2	1	2.5	2/10	4/10	2/6
6	2	3	5.5	2/22	4/22	2/6
6	2	5	8.5	2/34	4/17	2/6
6	3	1	3	3/9	3/9	3/6
6	3	2	5	3/15	3/15	3/6
6	3	4	9	3/27	3/27	3/6
6	4	1	4	4/8	2/8	4/6
6	4	3	10	4/20	2/20	4/6
6	4	5	16	4/32	2/32	4/6
6	5	0	1	5/1	1/1	5/6
6	5	1	7	5/7	1/7	5/6
6	5	2	13	5/13	1/13	5/6

[a]Length of packet as a fraction of segment length
[b]Length unoccupied is the length between packets as a fraction of segment length

that are in the appropriate division but lost in the elimination region. The first term can be broken up upon the observation that one division of the beam is prohibited from transmitting for every ($\phi-1$) divisions that are allowed to transmit, for a total of ϕ repeating divisions within a beam. This results in Equation (2) for the description of the length of the stable region.

$$l_{stable} = \frac{\phi(l_t + l_e) - (l_t + l_e)}{m} - l_e$$
$$= (\phi - 1)\frac{l_t + l_e}{m} - l_e \quad (2)$$

Extension to Higher Order Overtone Series

Equation (2) can be extended to higher order overtone series using the same argument. The overtone series index, k, describes to which higher order overtone series a peak belongs [23]. As described in the Supplemental Information, the number of divisions of the beam that are prohibited from transmitting are ($\phi-k$), with k divisions still transmitting. The Supplemental Information also provides the pattern that there are m ($\phi-k$) divisions within a segment, resulting in Equation (3) for l_{stable} including the effect of overtone series.

$$l_{stable} = \frac{\phi(l_t + l_e) - (\phi - k)(l_t + l_e)}{m(\phi - k)} - l_e$$
$$= k\frac{l_t + l_e}{m(\phi - k)} - l_e \quad (3)$$

Duty Cycle

From Equation (3), the stable region length of an individual packet decreases as the overtone increases. From the patterns seen in the Supplemental Information, we infer that the number of repeating packets within ϕ segments (a distance of ϕ $[l_t + l_e]$) is m ($\phi-k$), which yields the duty cycle described in Equation (4).

$$Duty\ Cycle = \frac{k(l_t + l_e) - m(\phi - k)l_e}{\phi(l_t + l_e)} \quad (4)$$

We define the duty cycle as the portion of the beam that overlaps transmitting packets when the mobility of the ions is perfectly matched to the field application frequency. Thus, the duty cycle is the maximum fractional peak height for a given set of conditions. We define the transmission efficiency as the portion of ions that transmit the drift tube, the actual peak height as a fraction of the ions entering the instrument. To go from duty cycle to transmission efficiency, the loss of ions due to diffusion must be considered. Typical these losses are due to axial diffusion and as such we will limit our discussion here to this phenomenon. As the packet size (effectively l_{stable}) decreases, it is more likely that a higher percentage of ions (particularly those near the center of the packet) will diffuse outside the stable packet length and be eliminated. We plot the transmission efficiency from the duty cycle with no diffusional losses as a function of overtone in Figure 3 and compare with simulated data. Simulations show a steeper drop off in signal compared with duty cycle equation, due to the aforementioned axial diffusion.

It is instructive to consider the duty cycle of IMS experiments as a comparison. In traditional IMS, the duty cycle is equal to the size of the packet (in time) divided by the time between injections. Conventional IMS and TWIMS have duty cycles of approximately 1 % [42]. In contrast, DMA and FAIMS instruments operate at steady state or effective steady state, respectively and, thus, have approximately 100 % duty cycle. The reader is reminded that in this work, duty cycle refers to the transmission of matched mobility ions and does not include any scan done for separation. In contrast to scanning techniques such as DMA, FAIMS, and OMS, the transmission efficiency of dispersive techniques, such as IMS and TWIMS, is typically above the

duty cycle. This relative increase in transmission efficiency is due to the development of ions traps before the drift tube and radial focusing at the end of the drift tube [10, 11]. Current work in our lab involves similar improvement of the transmission efficiency of OMS devices.

Maximum Overtone

Of note in the Figure 3 plots of duty cycle is the linear approach towards zero. From this it is obvious there must be a maximum overtone. The maximum OMS frequency coefficient is given in Equation (5), where allowable overtones are those corresponding to m with $l_{stable}>0$ and m_{max} corresponding to a transmitting packet size of zero. Observable overtones are those with $m<m_{max}$. We observed no signal even at overtones slightly below the maximum due to the small size of the transmitting packet; however, this boundary is not so firm as to preclude ions transmitting at particularly high ion counts, it just requires that they will have a distinct pattern of motion with different distances traveled in each phase.

$$m_{max} = \frac{k(l_t + l_e)}{l_e} \tag{5}$$

To better understand the maximum overtone it is informative to consider what happens to the packet size as it approaches and reaches this limit. Since each phase applied corresponds to an OMS frequency coefficient and each OMS frequency coefficient corresponds to a fractional distance through a segment, when m becomes large enough the distance moved is small enough that the packet does not even traverse the elimination region in few enough steps to avoid being eliminated by the appropriate applied phase. To relate this to the mathematical terms: for the primary series ($k=\phi-1$) of overtones, the maximum overtone is where the segment length (l_t+l_e) divided by the OMS frequency coefficient (m) has become as small or smaller than the length of the elimination region divided by the number of phases minus one ($\phi-1$). A similar result can be seen for the higher order overtone series.

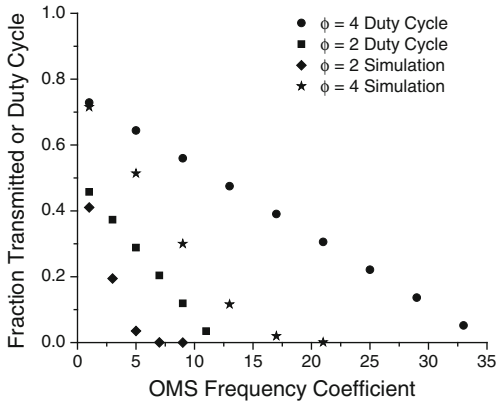

Figure 3. Duty cycle from Equation (4) and percent transmission from simulations as a function of overtone for the primary overtone series ($k=\phi-1$) for two- and four-phase OMS; m_{max} for this instrument according to Equation (5) is 11.8 for a two-phase system and 35.3 for a four-phase system

Comparison to Previous Experimental Results

Lee et al. [22] observed OMS frequency coefficients up to the 37 for the primary overtone series (k=3) of a four-phase system with l_t=5.6 cm and l_e=0.24 cm corresponding to an m_{max} of 73. With the same geometry, as used by Valentine et al. [21] for raffinose, for ϕ=2, 3, 4, 5, and 6, the maximum observed OMS frequency coefficient was 5, 7, 13, 16, and 19 whereas the maximum calculated OMS frequency coefficient is 24, 49, 73, 97, and 122. This discrepancy is expected because the previously described axial diffusion of mobility matched ions out of the transmitting packet increases as the packet decreases. This is in agreement with Figure 4 where increases in m and, therefore, decreases in l_{stable}, result in the ratio of transmission efficiency to the duty cycle to decrease. We expect to observe disparate numbers for maximum observed overtone and maximum calculated overtone in the original geometry because of the very high maximum overtone in this geometry; however, other geometries with longer elimination regions relative to the transmission region are likely to exhibit closer agreement between these maxima. In contrast, we observe that the circular instrument, an OMS-like device with an elimination region of approximately 30 cm and a transmission region of approximately 15 cm shows no overtones due to an m_{max} of 1.33 [43, 44]. In addition, all previous experimental results have shown decreasing signal as the overtone increases, as expected from the duty cycle shown in Equation (4) [20–24]. For simulations performed in this study we observe signal for all OMS frequency coefficients up to the 7th overtone for

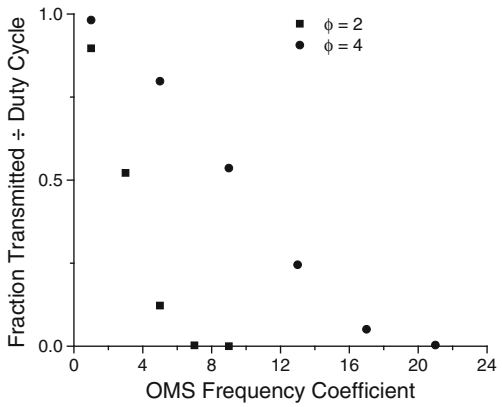

Figure 4. Simulated intensity over calculated duty cycle for two- and four-phase simulations to show the loss due to diffusion out of the transmitting packet along the axis of propagation

two-phase OMS, when m_{max} is 11.8, and we observe signal for all m up to the 21st with an m_{max} of 35.3.

Implications for Instrument Design

While not sufficient on their own, the derived equations are useful in understanding how to design new OMS instrumentation. In particular, the duty cycle and maximum overtone can be combined with previous equations for resolving power to provide insight into design constraints. Ignoring diffusion, the resolving power is proportional to the overtone OMS frequency coefficient times the number of segments and, thus, maximizing the observed overtone should maximize the resolving power for a given number of segments. If the number of segments and total instrument length are held constant, the length of the elimination region should be decreased to increase the maximum overtone. There is a limit to how small of an elimination region can be constructed; however, solutions can be found to engineer the elimination region small enough that the mean free path is now large compared to the instrument geometry and the conditions of ion mobility are no longer applicable as terminal velocity is no longer the primary mode of ion motion relative to the instrument geometry.

In contrast, if the length of the elimination region and the total length are held constant, there is a tradeoff between maximum overtone and the number of segments. Increasing the number of segments will decrease the length of the transmission region relative to the elimination region and, thus, decrease the maximum overtone. This tradeoff yields no significant change because the number of segments and maximum overtone are changed with the product remaining the same; instead the changes are subtle and these small differences ultimately require simulations in order to accurately and precisely compare potential instrument designs.

All of the above considerations assume that the driving force is to maximize resolving power. A requirement to increase signal suggests the use of an overtone below the maximum. From the equations we have derived above, we can better estimate the relative signal achieved by adjusting both the geometry and the overtone used. High overtones will clearly only be visible when the elimination region is small, the same condition desired for maximizing resolving power. Overall, the equations presented above should inform designers away from experimental designs that would have no signal because they are operated at overtones beyond the transmission limit.

Conclusions

Derivations of analytical expressions for the length of the transmitting packet and the length of the stable region, the duty cycle, and the maximum observable overtone for the OMS technique have been presented. These equations explain much of the loss of signal with increasing overtone seen in previous OMS experiments. Based upon these solutions, it appears that the shortest possible elimination region for a given segment length is ideal for obtaining maximum ion transmission and for maximizing resolving power.

Acknowledgments

The authors acknowledge partial support of this work provided by grants from the Analytical Node of the METACyt initiative funded by a grant from the Lilly Endowment and by the NIH (1RC1GM090798-01).

References

1. Valentine, S.J., Liu, X., Plasencia, M.D., Hilderbrand, A.E., Kurulugama, R.T., Koeniger, S.L., Clemmer, D.E.: Developing liquid chromatography ion mobility mass spectrometry techniques. *Expert Rev. Proteom.* **2**, 553–565 (2005)
2. McLean, J.A., Ruotolo, B.T., Gillig, K.J., Russell, D.H.: Ion mobility-mass spectrometry: A new paradigm for proteomics *Int. J. Mass Spectrom.* **240**, 301–315 (2005)
3. Isailovic, D., Kurulugama, R.T., Plasencia, M.D., Stokes, S.T., Kyselova, Z., Goldman, R., Mechref, Y., Novotny, M.V., Clemmer, D.E.: Profiling of human serum glycans associated with liver cancer and cirrhosis by IMS-MS. *J. Proteome Res.* **7**, 1109–1117 (2008)
4. Williams, J.P., Grabenauer, M., Holland, R.J., Carpenter, C.J., Wormald, M.R., Giles, K., Harvey, D.J., Bateman, R.H., Scrivens, J.H., Bowers, M.T.: Characterization of simple isomeric oligosaccharides and the rapid separation of glycan mixtures by ion mobility mass spectrometry. *Int. J. Mass Spectrom.* **298**, 119–127 (2010)
5. Li, Z., Valentine, S.J., Clemmer, D.E.: Complexation of amino compounds by 18C6 improves selectivity by IMS-IMS-MS: Application to petroleum characterization. *J. Am. Soc. Mass Spectrom.* **22**, 817–827 (2011)
6. Becker, C., Fernandez-Lima, F.A., Russell, D.H.: Ion mobility-mass spectrometry: A tool for characterizing the petroleome. *Spectroscopy* **24**, 38–42 (2009)
7. Bernstein, S.L., Duipuis, N.F., Lazo, N.D., Wyttenbach, T., Condron, M.M., Bitan, G., Teplow, D.B., Shea, J.-E., Ruotolo, B.T., Robinson, C.V., Bowers, M.T.: Amyloid-β protein oligomerization and the importance of tetramers and dodecamers in the aetiology of Alzheimer's disease. *Nat. Chem.* **1**, 326–331 (2009)
8. Uetrecht, C., Barbu, I.M., Shoemaker, G.K., van Duijn, E., Heck, A.J.R.: Interrogating viral capsid assembly with ion mobility-mass spectrometry. *Nat. Chem.* **3**, 126–132 (2011)
9. Giles, K., Pringle, S.D., Worthington, K.R., Little, D., Wildgoose, J.L., Bateman, R.H.: Applications of a traveling wave-based radio-frequency only stacked ring ion guide. *Rapid Commun. Mass Spectrom.* **18**, 2401–2414 (2004)
10. Pringle, S.D., Giles, K., Wildgoose, J.L., Williams, J.P., Slade, S.E., Thalassinos, K., Bateman, R.H., Bowers, M.T., Scrivens, J.H.: An investigation of the mobility separation of some peptide and protein ions using a new hybrid quadrupole/traveling wave IMS/oa-TOF instrument. *Int. J. Mass Spectrom.* **261**, 1–12 (2007)
11. Shvartsburg, A.A., Smith, R.D.: Fundamentals of traveling wave ion mobility spectrometry. *Anal. Chem.* **80**, 9689–9699 (2008)
12. Giles, K., Williams, J.P., Campuzano, I.: Enhancements in traveling wave ion mobility resolution. *Rapid Commun. Mass Spectrom.* **25**, 1559–1566 (2011)
13. Rosell-Llompart, J., Loscertales, J.G., Bingham, D., Fernandez de la Mora, J.: Sizing nanoparticles and ions with a short differential mobility analyzer. *J. Aerosol Sci.* **27**, 695–719 (1996)
14. Kaufman, S.L., Skogen, J.W., Dorman, F.D., Zarrin, F., Lewis, K.C.: Macromolecule analysis based on electrophoretic mobility in air: Globular proteins. *Anal. Chem.* **68**, 1895–1904 (1996)
15. Kaddis, C.S., Lomeli, S.H., Yin, S., Berhane, B., Apostol, M.I., Kickhoefer, V.A., Rome, L.H., Loo, J.A.: Sizing large proteins and

protein complexes by electrospray ionization mass spectrometry and ion mobility. *J. Am. Soc. Mass Spectrom.* **18**, 1206–1216 (2007)
16. Gorshkov, M.P.: USSR Inventory's Certificate 966583, (1982)
17. Purves, R.W., Guevremont, R., Day, S., Pipich, C.W., Matyjaszczyk, M.S.: Mass spectrometric characterization of a high-field asymmetric waveform ion mobility spectrometer. *Rev. Sci. Instrum.* **69**, 4094–4105 (1998)
18. Shvartsburg, A.A., Tang, K., Smith, R.D.: Understanding and designing field asymmetric waveform ion mobility spectrometry separations in gas mixtures. *Anal. Chem.* **76**, 7366–7374 (2004)
19. Shvartsburg, A.A., Prior, D.C., Tang, K., Smith, R.D.: High-resolution differential ion mobility separations using planar analyzers at elevated dispersion fields. *Anal. Chem.* **82**, 7649–7655 (2010)
20. Kurulugama, R., Nachtigall, F.M., Lee, S., Valentine, S.J., Clemmer, D.E.: Overtone mobility spectrometry: Part 1. Experimental observations. *J. Am. Soc. Mass Spectrom.* **20**, 729–737 (2009)
21. Valentine, S.J., Stokes, S.T., Kurulugama, R.T., Nachtigall, F.M., Clemmer, D.E.: Overtone mobility spectrometry: Part 2. Theoretical considerations of resolving power. *J. Am. Soc. Mass Spectrom.* **20**, 738–750 (2009)
22. Lee, S., Ewing, M.A., Nachtigall, F.M., Kurulugama, R.T., Valentine, S.J., Clemmer, D.E.: Determination of cross sections by overtone mobility spectrometry: Evidence for loss of unstable structures at higher overtones. *J. Phys. Chem. B* **114**, 12406–12415 (2010)
23. Valentine, S.J., Kurulugama, R.T., Clemmer, D.E.: Overtone mobility spectrometry: Part 3. On the origin of peaks. *J. Am. Soc. Mass Spectrom.* **22**, 804–816 (2011)
24. Kurulugama, R.T., Nachtigall, F.M., Valentine, S.J., Clemmer, D.E.: Overtone mobility spectrometry: Part 4. OMS-OMS analyses of complex mixtures. *J. Am. Soc. Mass Spectrom.* **22**, 2049–2060 (2011)
25. Tyndall, A.M.: The Mobility of Positive Ions in Gases. Cambridge University Press, Cambridge (1938)
26. Mason, E.A., McDaniel, E.W.: Transport Properties of Ions in Gases, pp. 1–27, 137–223. Wiley, New York (1988)
27. Revercomb, H.E., Mason, E.A.: Theory of plasma chromatography/gaseous electrophoresis—a review. *Anal. Chem.* **47**, 970–983 (1975)
28. St. Louis, R.H., Hill Jr., H.H., Eiceman, G.A.: Ion mobility spectrometry in analytical chemistry. *Crit. Rev. Anal. Chem.* **21**, 321–355 (1990)
29. Clemmer, D.E., Jarrold, M.F.: Ion mobility measurements and their applications to clusters and biomolecules. *J. Mass Spectrom.* **32**, 577–592 (1997)
30. Kanu, A.B., Dwivedi, P., Tam, M., Matz, L., Hill Jr., H.H.: Ion mobility-mass spectrometry. *J. Mass Spectrom.* **43**, 1–22 (2008)
31. Hoaglund-Hyzer, C.S., Counterman, A.E., Clemmer, D.E.: Anhydrous protein ions. *Chem. Rev.* **99**, 3037–3079 (1999)
32. Wyttenbach, T., von Helden, G., Batka Jr., J.J., Carlat, D., Bowers, M.T.: Effect of the long-range potential on ion mobility measurements. *J. Am. Soc. Mass Spectrom.* **8**, 275–282 (1997)
33. Shvartsburg, A.A., Jarrold, M.F.: An exact hard spheres scattering model for the mobility of polyatomic ions. *Chem. Phys. Lett.* **261**, 86–91 (1996)
34. Mesleh, M.F., Hunter, J.M., Shvartsburg, A.A., Schatz, G.C., Jarrold, M.F.: Structural information from ion mobility measurements: effects of the long range potential. *J. Phys. Chem.* **100**, 16082–16086 (1996). Erratum: *J. Phys. Chem. A*. **101**, 968 (1997)
35. Bluhm, B.K., Gillig, K.J., Russell, D.H.: Development of a Fourier-transform ion cyclotron resonance mass spectrometer-ion mobility spectrometer. **71**, 4078–4086 (2000)
36. Tang, K., Shvartsburg, A.A., Lee, H.-N., Prior, D.C., Buschbach, M.A., Li, F., Tolmachev, A.V., Anderson, G.A., Smith, R.D.: High-sensitivity ion mobility spectrometry/mass spectrometry using electrodynamic ion funnel interfaces. *Anal. Chem*. **77**, 3330–3339 (2005)
37. Koeniger, S.L., Merenbloom, S.I., Valentine, S.J., Jarrold, M.F., Udseth, H.R., Smith, R.D., Clemmer, D.E.: An IMS-IMS analogue of MS-MS. *Anal. Chem.* **78**, 4161–4174 (2006)
38. Appelhans, D.A., Dahl, D.A.: SIMION ion optics simulations at atmospheric pressure. *Int. J. Mass Spectrom.* **244**, 1–14 (2005)
39. Julian, R.R., Mabbett, S.R., Jarrold, M.F.: Ion funnels for the masses: Experiments and simulations with a simplified ion funnel. *J. Am. Soc. Mass Spectrom.* **16**, 1708–1712 (2005)
40. Scientific Instrument Services Inc.: SIMION ver. 8.0, Ringoes, NJ, USA
41. Myung, S., Lee, Y.J., Moon, M.H., Taraszka, J., Sowell, R., Koeniger, S., Hilderbrand, A.E., Valentine, S.J., Cherbas, L., Cherbas, P., Kaufmann, T.C., Miller, D.F., Mechref, Y., Novotny, M.V., Ewing, M.A., Sporleder, C.R., Clemmer, D.E.: Development of high-sensitivity ion trap ion mobility spectrometry time-of-flight techniques: A high-throughput Nano-LC-IMS-TOF separation of peptides arising from a *Drosophila* protein extract. *Anal. Chem.* **75**, 5137–5145 (2003)
42. Liu, Y., Valentine, S.J., Counterman, A.E., Hoaglund, C.S., Clemmer, D.E.: Injected-ion mobility analysis of biomolecules. *Anal. Chem.* **69**, 728A–735A (1997)
43. Merenbloom, S.I., Glaskin, R.S., Henson, Z.B., Clemmer, D.E.: High resolution ion cyclotron mobility spectrometry. *Anal. Chem.* **81**, 1482–1487 (2009)
44. Glaskin, R.S., Valentine, S.J., Clemmer, D.E.: A scanning mode for ion cyclotron mobility spectrometry. *Anal. Chem.* **82**, 8266–8271 (2010)